Particle method of characteristics (PMOC) for unsteady pipe flow

Yao-Hsin Hwang, Ho-Shuenn Huang, Nien-Mien Chung and Pai-Yi Wang

ABSTRACT

A novel particle method of characteristics (PMOC) to simulate unsteady pipe flows is introduced and validated in the present study. Contrary to the conventional method of characteristics (MOC), the present formulation is built by reallocating the computational nodes along the characteristic lines. Both the right- and left-running characteristics are accurately traced and imitated with their associated computational particles. The annoying numerical inconveniences in the fixed-grid arrangement due to incompatible Courant–Friedrichs–Lewy (CFL) condition by repeating solution interpolations is effectively eliminated. Special particles with dual states satisfying the Rankine–Hugoniot relations are deliberately imposed to emulate the shock structure. Efficacy of this formulation is verified by solving some benchmark problems with significant transient effects in pipe flows. Computational results of piezometric head and flow velocity are meticulously compared with available analytical solutions. It is concluded that the proposed PMOC will be a useful tool to replicate transient phenomena in pipe flows.

Key words | particle method of characteristics, Rankine–Hugoniot relation, shock particle, transient pipe flow

Yao-Hsin Hwang
Department of Marine Engineering,
National Kaohsiung Marine University,
Kaohsiung 80543,
Taiwan

Ho-Shuenn Huang (corresponding author)
Department of Naval Architecture and Ocean Engineering,
National Kaohsiung Marine University,
Kaohsiung 81143,
Taiwan
E-mail: *hoshuenn@webmail.nkmu.edu.tw*

Nien-Mien Chung
Pai-Yi Wang
Taiwan Power Research Institute,
Taiwan Power Company,
Taipei 23847,
Taiwan

INTRODUCTION

Transient flow is an important phenomenon in safety operations of piping systems. Abrupt pressure change in the pipeline may bring on severe failure of hydraulic devices. It is thus a crucial issue to have an accurate prediction on the behavior of transient flows. Of the available numerical methodologies to simulate pressure propagation (Chaudhry 1987; Wylie & Streeter 1993), the method of characteristics (MOC) has gained noteworthy popularity in engineering practices for its simplicity in coding, efficiency, and accuracy. Indeed, MOC has been incorporated in many existing engineering software packages as a kernel operator to predict transient phenomena in piping systems (Ghidaoui *et al.* 2005). To carry out an MOC analysis, the related partial differential equations are transformed into ordinary ones which can then be integrated along their respective characteristic lines (Lister 1960; Abbott 1966; Chaudhry 1987; Lai 1988; Wylie & Streeter 1993). The coupled equation system can therefore be traced with these simplified compatibility equations. Numerical inaccuracy in imitating information transmission can be effectively alleviated as long as the adopted grid spacing and time step comply with the Courant condition. However, in the cases of multiple reaches or with varying wave celerity, it may be impractical to fulfill the Courant condition with the given computational nodes and specified time interval for all pipe branches. This is the so-called Courant–Friedrichs–Lewy (CFL) limitation adherent to the method of fixed time interval or fixed-grid method. Approximation via solution interpolation will be indispensible to proceed with the computation and consequently deteriorates the simulation accuracy due to its inherent numerical errors (van Leer 1973; Wiggert & Sundquist 1977; Goldberg & Wylie 1983; Sibertheros *et al.* 1991; Yang & Hsu 1991; Ghidaoui & Karney 1994).

To avoid the numerical inaccuracy brought in by the solution interpolation procedures, one may employ the characteristic-grid (CG) where the locations of

doi: 10.2166/hydro.2012.116

computational nodes are arranged to yield a unity Courant number regardless of local flow condition. The computational nodes are located at the intersection points of characteristic lines from different families in the spatial-temporal $(x-t)$ plane. Thus the locations of computational nodes become a part of the solution and it is not possible to assign their positions exactly at the prescribed times in advance. Results are not directly available at a particular instant along the pipe, neither is it possible to introduce boundary conditions at predefined times. Further interpolations and/or adjustment of computational nodes are required although the introduced numerical damping effect is not nearly as significant as a fixed-grid MOC (Tullis *et al.* 1976; Wylie & Streeter 1976).

Besides the above-mentioned computational obstacles, all conventional MOC based on compatibility equations suffer from the inability to secure a feasible solution when two characteristic lines of the same family converge. It is the usual scenario when the flow convection effect is substantial or the variation in wave celerity is not negligible. The results of calculation obtained by MOC will be questionable since the transmitted characteristics become multi-valued. Physically, a shock comes into existence in this circumstance. A single-state computational node is insufficient to reveal the proper solution attributes across a shock. In fact, the compatibility equations must be discarded and substituted by the Rankine–Hugoniot relation to accommodate possible solution jump (Shapiro 1953). Accordingly, a multi-state computational node will be essential to depict the intricacy associated with an admissible shock.

The objective of the present study is to introduce and validate a novel numerical scheme to resolve the transient phenomena in pipe flows. It is also built upon the compatibility equations as in MOC. However, the computational nodes are reallocated to follow the characteristic lines such that the numerical obstacle for the CFL limitation can be got rid of. Furthermore, unlike the CG arrangement, our computations can be implemented at any specified time without superfluous interpolation on the transmitted characteristics. With this peculiar mobility of computational nodes, the present formulation can be coined as a particle method of characteristics (PMOC) to distinguish it from the conventional ones. Individual characteristics are accurately traced and imitated by their respective computational particles along the associated characteristic lines. Therefore, there are two groups of particles to tackle the unsteady features in pipe flows. The right-running particle is employed to deal with the right-running characteristic and left-running particle with left-running characteristic. Meanwhile, commencement of a shock can be identified as two particles in the same group colliding, which is in accordance with the intersection of two characteristic lines. Once a shock is detected, a particular particle with dual states is imposed to mimic its intricacy. These states are deduced from the fulfillment of Rankine–Hugoniot relation across a shock. The shock structure and its subsequent evolution can then be accurately coped with. In this sense, this particle is designated a shock particle. On the other hand, those following characteristic lines to sort out the compatibility equations are regarded as regular ones. It is worth noting that the present methodology is formulated to resolve flow features along the characteristic lines rather than the streamlines used in a conventional particle method (Gingold & Monaghan 1977; Hwang 2011).

Validation of the present formulation is conducted by solving some benchmark problems with significant transient effects in pipe flows. Those with negligible nonlinear convection terms suggested by Sobey (2002, 2004) are considered to verify the feasibility of the proposed PMOC in the simplified situation. Numerical results are directly compared with available analytical solutions. Subsequently, cases with significant convection terms are considered by solving some shock-tube problems with various wave patterns. Both shock and expansion waves are taken into account in this category. They cannot be accurately resolved by the conventional MOC or linearization analysis. It will demonstrate the ability of the present proposition in mimicking the evolvements of wave patterns. Comparisons with exact solutions are also performed to depict its accuracy.

CHARACTERISTICS OF TRANSIENT PIPE FLOW

In this section, governing equations and their essential features required for the present formulation are briefly outlined. It emphasizes the transmitting characteristics in the governing equations and Rankine–Hugoniot relations

to depict an admissible shock. Numerical treatments for these equations will be detailed in the next section.

Governing equations

The continuity and momentum equations of describing flow transient phenomena in a horizontal pipeline can be summarized as follows (Chaudhry 1987; Wylie & Streeter 1993):

$$\frac{\partial H}{\partial \tau} + V\frac{\partial H}{\partial X} + \frac{a^2}{g}\frac{\partial V}{\partial X} = 0 \tag{1a}$$

$$\frac{\partial V}{\partial \tau} + V\frac{\partial V}{\partial X} + g\frac{\partial H}{\partial X} + J = 0 \tag{1b}$$

where τ is a temporal variable, X is the spatial variable, H is flow piezometric head, V is the cross-sectional averaged velocity, a is the wave transmitting speed, g is the gravitational acceleration, and J accounts for the friction term. In a circular pipe, the wave transmitting speed a can be derived as:

$$a = \sqrt{\frac{K/\rho}{1 + (K/E)(D/e)}} \tag{2}$$

where ρ is the fluid density, K is bulk modulus of elasticity of the fluid, E is the Young's modulus of elasticity for the pipe, D and e are the diameter and thickness of the pipe, respectively. It is noted that the nonlinear flow convection terms (i.e., $V(\partial H/\partial X)$ and $V(\partial V/\partial X)$) are retained in these governing equations.

The friction term J can be estimated by the Darcy–Weisbach model:

$$J = \frac{f|V|}{2D}V \tag{3a}$$

where f is the Darcy–Weisbach friction factor. For comparison with the linearized exact solution (Sobey 2004), this friction term is further simplified by the following linear form:

$$J = \Lambda V \tag{3b}$$

As noted by Sobey (2004), the quadratic expression in Equation (3a) is still not entirely satisfactory and the utility of the linear approximation can be enhanced by realistic estimates of Λ. However, it is noted that the original quadratic model in Equation (3a) can be easily taken up in the present numerical treatment.

For convenience, the governing Equation system (1) is normalized with

$$t = a\tau/L,\ x = X/L,\ h = Hg/a^2,\ v = V/a,\ \text{and}\ \lambda = \Lambda L/a \tag{4}$$

to yield its dimensionless counterpart:

$$\frac{\partial h}{\partial t} + v\frac{\partial h}{\partial x} + \frac{\partial v}{\partial x} = 0 \tag{5a}$$

$$\frac{\partial v}{\partial t} + \frac{\partial h}{\partial x} + v\frac{\partial v}{\partial x} = -\lambda v \tag{5b}$$

In the normalization procedure, L is the reference pipe length. This dimensionless Equation system (5) can then be equivalently expressed in a vector form:

$$\frac{\partial \boldsymbol{V}}{\partial t} + \boldsymbol{A}\frac{\partial \boldsymbol{V}}{\partial x} = \boldsymbol{S} \tag{6}$$

with the following solution vector $\boldsymbol{V}$, coefficient matrix $\boldsymbol{A}$, and source vector $\boldsymbol{S}$:

$$\boldsymbol{V} = \begin{pmatrix} h \\ v \end{pmatrix},\quad \boldsymbol{A} = \begin{pmatrix} v & 1 \\ 1 & v \end{pmatrix},\quad \text{and}\quad \boldsymbol{S} = \begin{pmatrix} 0 \\ -\lambda v \end{pmatrix}.$$

In the above and subsequent equations in this article, the boldface letters are employed to represent the vector or matrix quantities. Although the present formulation concerns the simulation of transients in a horizontal pipe, it can be applied to describe those in a sloping pipe without serious difficulty. Indeed, effects in a sloping pipe can be taken into account by incorporating an additional source term in the governing equations. Essential features of the equation characteristics revealed in the present study are still applicable.

Characteristic analyses

The present particle method is also formulated on the characteristics of flow equations. Detailed descriptions on the characteristics of an equation system, Equations (5) or (6),

can be found in the existing literature (Chaudhry 1987; Hirsch 1990; Wylie & Streeter 1993; LeVeque 2002). Therefore, they are briefly summarized in this section for reference. First, the coefficient matrix $\boldsymbol{A}$ can be diagonalized as:

$$\boldsymbol{A} = \boldsymbol{R}\boldsymbol{D}\boldsymbol{R}^{-1} \tag{7}$$

with the right-side eigenvector $\boldsymbol{R}$ and diagonal matrices $\boldsymbol{D}$:

$$\boldsymbol{R} = \frac{1}{\sqrt{2}}\begin{pmatrix} 1 & 1 \\ 1 & -1 \end{pmatrix} \quad \text{and} \quad \boldsymbol{D} = \begin{pmatrix} v+1 & 0 \\ 0 & v-1 \end{pmatrix}$$

respectively. The Equation system (6) can then be rearranged as:

$$\boldsymbol{R}^{-1}\frac{\partial \boldsymbol{V}}{\partial t} + \boldsymbol{D}\boldsymbol{R}^{-1}\frac{\partial \boldsymbol{V}}{\partial x} = \boldsymbol{R}^{-1}\boldsymbol{S} \tag{8a}$$

or, equivalently

$$\frac{\partial \boldsymbol{W}}{\partial t} + \boldsymbol{D}\frac{\partial \boldsymbol{W}}{\partial x} = \boldsymbol{R}^{-1}\boldsymbol{S} \tag{8b}$$

It is interesting to note that $\boldsymbol{R}^{-1} = \boldsymbol{R}$ in this case. The above Equation (8b) introduces two relevant characteristic variables:

$$\boldsymbol{W} = \begin{pmatrix} w^+ \\ w^- \end{pmatrix} = \boldsymbol{R}^{-1}\boldsymbol{V} = \begin{pmatrix} (h+v)/\sqrt{2} \\ (h-v)/\sqrt{2} \end{pmatrix} \tag{9a}$$

Conversely, the solution variables (h, v) can be obtained from the characteristic ones:

$$\boldsymbol{V} = \begin{pmatrix} h \\ v \end{pmatrix} = \boldsymbol{R}\boldsymbol{W} = \begin{pmatrix} (w^+ + w^-)/\sqrt{2} \\ (w^+ - w^-)/\sqrt{2} \end{pmatrix} \tag{9b}$$

Furthermore, the source term in the right-hand side of Equation (8) becomes:

$$\boldsymbol{R}^{-1}\boldsymbol{S} = \begin{pmatrix} -\lambda v/\sqrt{2} \\ \lambda v/\sqrt{2} \end{pmatrix} = \begin{pmatrix} -\lambda(w^+ - w^-)/\sqrt{2} \\ \lambda(w^+ - w^-)/\sqrt{2} \end{pmatrix} \tag{10}$$

Associated with the above relations, the governing equations expressed in characteristic form, Equation (8), can be arranged as:

$$\frac{\partial w^+}{\partial t} + (v+1)\frac{\partial w^+}{\partial x} = -\lambda(w^+ - w^-)/\sqrt{2} \tag{11a}$$

$$\frac{\partial w^-}{\partial t} + (v-1)\frac{\partial w^-}{\partial x} = \lambda(w^+ - w^-)/\sqrt{2} \tag{11b}$$

Physically, they can be interpreted as the compatibility equations along their corresponding characteristic lines:

(i) Along the characteristic line of:

$$\frac{dx}{dt} = v + 1 = c^+,\ \frac{dw^+}{dt} + \frac{\lambda}{\sqrt{2}}w^+ = \frac{\lambda}{\sqrt{2}}w^- \tag{12a}$$

(ii) Along the characteristic line of:

$$\frac{dx}{dt} = v - 1 = c^-,\ \frac{dw^-}{dt} + \frac{\lambda}{\sqrt{2}}w^- = \frac{\lambda}{\sqrt{2}}w^+ \tag{12b}$$

In this way, the original partial differential Equation system (5) is transferred into an ordinary one along the characteristic lines. For distinction, the first one with $dx/dt = c^+$ is regarded as the right-running characteristic and the second one with $dx/dt = c^-$ the left-running one (the wave celerity, $c^+ > c^-$). Meanwhile, superscripts + and − are employed to signify the right- and left-running characteristics, respectively. These compatibility equations are the bedrock for the MOC.

It must be emphasized that the propagation of characteristic lines will depend upon the local flow condition. They may be divaricating to form expansion fans or agglomerated to shocks. In the latter case, the characteristic lines will merge together such that it becomes impractical to determine a unique characteristic at the shock location. Therefore, the relationship in Equation (12) fails to describe the flow evolution and it must be substituted by the Rankine–Hugoniot relation to link the states across a shock (Shapiro 1953).

Rankine–Hugoniot relation

The Rankine–Hugoniot relation is proposed by accommodating solution discontinuity to yield a plausible calculation. For practice, the differential governing Equations (5a) and (5b) must be rearranged with their conservative form:

$$\frac{\partial \boldsymbol{U}}{\partial t}+\frac{\partial \boldsymbol{F}}{\partial x}=e^{h}\boldsymbol{S} \tag{13a}$$

with the associated conserved variables and flux functions:

$$\boldsymbol{U}=\begin{pmatrix} e^{h} \\ e^{h}v \end{pmatrix} \quad \text{and} \quad \boldsymbol{F}=\begin{pmatrix} e^{h}v \\ e^{h}v^{2}+e^{h} \end{pmatrix}. \tag{13b}$$

This equation system can be integrated over a region with solution jump. With the control element lifetime locus depicted in Figure 1, its consequential integral form reads:

$$(\boldsymbol{U}_L-\boldsymbol{U}_R)\delta x+[\boldsymbol{F}(U_R)-\boldsymbol{F}(U_L)]\delta t=e^{\bar{h}}\bar{\boldsymbol{S}}\delta x\delta t$$

where $e^{\bar{h}}\bar{\boldsymbol{S}}$ is the average values of $e^{h}\boldsymbol{S}$ in the control volume. By taking the limit of infinitesimal control volume (δx, $\delta t \to 0$), the above equation becomes:

$$\sigma(\boldsymbol{U}_L-\boldsymbol{U}_R)=\boldsymbol{F}(\boldsymbol{U}_L)-\boldsymbol{F}(\boldsymbol{U}_R) \tag{14a}$$

or, in the componentwise expression

$$\sigma(e^{h_L}-e^{h_R})=e^{h_L}v_L-e^{h_R}v_R \tag{14b}$$

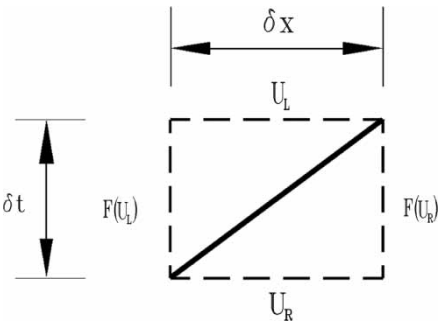

Figure 1 | Control element lifetime locus for a moving shock.

$$\sigma(e^{h_L}v_L-e^{h_R}v_R)=e^{h_L}v_L^{2}+e^{h_L}-e^{h_R}v_R^{2}-e^{h_R} \tag{14c}$$

where σ is the shock speed with $\sigma=\delta x/\delta t$, and the subscripts L and R, respectively, denote the left and right sides of a shock. Accordingly, the Rankine–Hugoniot relation can be derived from Equations (14b) and (14c) after eliminating the shock speed:

$$[e^{(h_L-h_R)/2}-e^{-(h_L-h_R)/2}]^{2}=(v_L-v_R)^{2}$$

That is, a shock sustains if the above relation is satisfied. For computational convenience, this relation can be further generalized in the account of right- and left-running shocks:

$$\eta+\sinh(\eta)=m \tag{15a}$$

with

$$[\eta, m]=\begin{cases} [(h_L-h_R)/2, (w_L^{+}-w_R^{+})/\sqrt{2}] & \textit{for a right-running shock} \\ [(h_R-h_L)/2, (w_R^{-}-w_L^{-})/\sqrt{2}] & \textit{for a left-running shock} \end{cases} \tag{15b}$$

The right- and left-running shocks are formed from the amalgamation of right- and left-running characteristic lines, respectively. It is worth noting that a plausible shock exists only for $m>0$. It is the direct consequence of $h_L>h_R$ and $h_L<h_R$ for a right- and left-running shock, respectively. In this expression, η is directly related to the piezometric head difference across a shock and m can be considered as a shock strength indicator.

As shown in Equation (15), the Rankine–Hugoniot relation is a nonlinear equation which needs an appropriate iterative scheme to yield a converged solution. A practical initial guess will be helpful to secure an efficient solution:

$$\eta_0=\frac{m}{2}\left(1-\frac{m^{2}}{48+3m^{2}}\right) \tag{16}$$

This estimation is deduced from the approximation of $\eta+\sinh(\eta)\approx 2\eta+\eta^{3}/6$ for Equation (15). In general, it can yield solution residual less than 2×10^{-8} for $m\le 0.15$. In addition, only three iterations are required for $m=2$

with the Newton–Raphson method (Carnaha *et al.* 1969) to drive the equation residual to machine zero (less than 10^{-16} in our calculations).

NUMERICAL TREATMENT

In this section, we will describe the numerical tactics adopted in the present study to solve the governing Equations (1) or (5). Since a shock may emerge in the solution procedure, both the regular and shock particles must be taken into consideration for a feasible numerical simulation.

Regular particles

As depicted in Equations (12a) and (12b), there are two types of characteristic lines with their corresponding compatibility equations to render the flow evolution. It is a natural preference by adopting two groups of computational particles in tracking the associated characteristics. These particles are maneuvered to move along their associated characteristic lines. The corresponding flow characteristics are updated according to the discrete expressions for compatibility equations:

(i) For the right-running characteristic,

$$x_{p^+}^{n+1} = x_{p^+}^{n} + (v_{p^+}^{n} + 1)\Delta t \quad \text{and}$$
$$w_{p^+}^{+,n+1} = (w_{p^+}^{+,n} - w_{p^+}^{-,n})e^{-\lambda\Delta t/\sqrt{2}} + w_{p^+}^{-,n}; \tag{17a}$$

(ii) For the left-running characteristic,

$$x_{p^-}^{n+1} = x_{p^-}^{n} + (v_{p^-}^{n} - 1)\Delta t \quad \text{and}$$
$$w_{p^-}^{-,n+1} = (w_{p^-}^{-,n} - w_{p^-}^{+,n})e^{-\lambda\Delta t/\sqrt{2}} + w_{p^-}^{+,n} \tag{17b}$$

In these equations, superscript n and $n+1$, respectively, denote the computational results at previous and current steps; Δt is the time step, and subscripts p^+ and p^- are employed to signify the right- and left-running computational particles, respectively. That is, the right-running (p^+) and left-running (p^-) particles are managed to move along the right- and left-running characteristic lines, respectively. In this manner, the right-running characteristic of a right-running node is updated by Equation (17a) and the left-running characteristic of a left-running node by Equation (17b). For convenience, these characteristics are regarded as the transmitted characteristics. In the case of negligible friction term (i.e., $\lambda = 0$), Equations (17a) and (17b) can be reduced as $w_{p^+}^{+,n+1} = w_{p^+}^{+,n}$ and $w_{p^-}^{-,n+1} = w_{p^-}^{-,n}$, respectively. It implies the transmitted characteristics will remain unchanged along their associated characteristic lines. Finally, it should be noted that the discrete counterpart for updating the transmitted characteristics is derived by the direct integration of compatibility equations while assuming the variations in $w_{p^+}^{-,n}$ and $w_{p^-}^{+,n}$ are negligible. Nevertheless, it will yield an unconditionally stable prediction regardless of the adopted time step.

Besides the transmitted characteristics, another solution variable is required to settle down the solution state at a typical computational particle. It is the left-running characteristic for a right-running particle ($w_{p^+}^{-}$) and right-running characteristic for a left-running particle ($w_{p^-}^{+}$). Since a right-running particle may not happen to be coincident with a left-running particle, these quantities must be interpolated from the secured transmitted ones. As shown in Figure 2(a), the left-running characteristic for a right-running particle ($w_{p^+}^{-}$) is deduced with a linear approximation between two successive left-running ones ($w_{p^-}^{-}$):

$$w_{p^+}^{-,n+1} = \frac{x_{R^-}^{n+1} - x_{p^+}^{n+1}}{x_{R^-}^{n+1} - x_{L^-}^{n+1}} w_{L^-}^{-,n+1} + \frac{x_{p^+}^{n+1} - x_{L^-}^{n+1}}{x_{R^-}^{n+1} - x_{L^-}^{n+1}} w_{R^-}^{-,n+1}. \tag{18a}$$

Similarly, as shown in Figure 2(b), the right-running characteristic for a left-running particle ($w_{p^-}^{+}$) becomes:

$$w_{p^-}^{+,n+1} = \frac{x_{R^+}^{n+1} - x_{p^-}^{n+1}}{x_{R^+}^{n+1} - x_{L^+}^{n+1}} w_{L^+}^{+,n+1} + \frac{x_{p^-}^{n+1} - x_{L^+}^{n+1}}{x_{R^+}^{n+1} - x_{L^+}^{n+1}} w_{R^+}^{+,n+1}. \tag{18b}$$

Because the transmitted characteristics are directly derived from the compatibility equations, these interpolations will not induce serious numerical error such as that in a conventional MOC. Indeed, the accuracy of the transmitted characteristics will not be contaminated by these

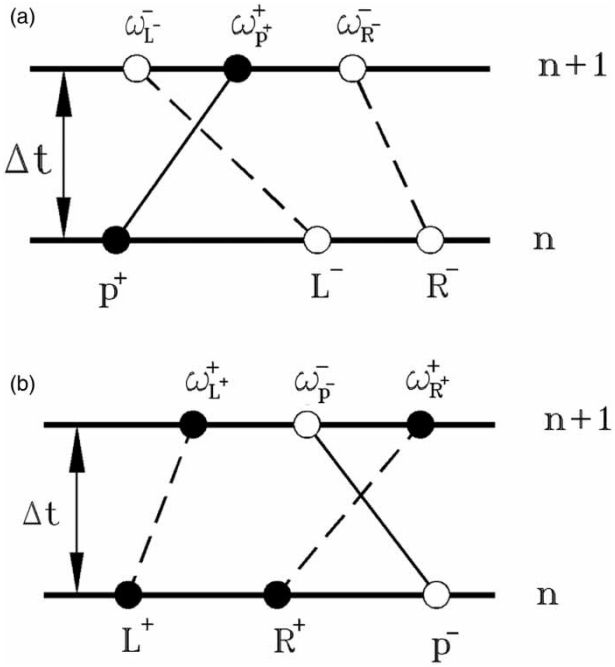

Figure 2 | Interactions of characteristic node. (a) Right-running characteristic node; (b) Left-running characteristic node.

interpolations. For discrimination, those obtained by interpolation from the transmitted ones can be denoted as the interpolated characteristics. Therefore, the complete state of a computational particle is specified by its transmitted and interpolated characteristics.

From the above derivations, the present formulation is distinguished from the convectional MOC by which their special features affix to the computational nodes. The present formulation consists of two types of computational particles while the conventional one adopts a single type. The computational nodes are movable in the present formulation while they are stationary in a conventional MOC. Therefore, it can be designated as an active MOC since the computational nodes tackle the characteristics in an active manner. Numerical CFL limitation in the fixed-grid MOC can be completely eradicated without deteriorating the simulation accuracy. Furthermore, the methodology introduced in the present formulation can be applied to resolve equation systems equipped with more characteristics without serious difficulties. It is not a trivial task to extend the conventional MOC for problems with more that two characteristics. It is also impractical to demand that all characteristic lines from different families should intersect at the computational nodes.

Shock particles

One of the essential drawbacks of the conventional MOC is its incapability to accurately simulate a strong pressure wave, especially accompanied with a shock. The shock is formed by the agglomeration of characteristic lines and, as a consequence, there does not exist a unique characteristic line to track the transmitted characteristics. Meanwhile, multiple states must be considered for an accurate representation of the shock structure. These issues cannot be easily resolved with the conventional fixed-grid MOC. However, in our present formulation, the characteristic lines can be palpably delineated by the moving computational particles. It provides a simple scheme to specify the formation location of a plausible shock. As illustrated in Figure 3(a), a shock comes into existence if two successive computational particles collide:

$$x^n_{L^\pm} + (v^n_{L^\pm} \pm 1)\Delta t = x^n_{R^\pm} + (v^n_{R^\pm} \pm 1)\Delta t \tag{19a}$$

which is applicable for both the right- and left-running characteristic particles. In fact, it is also related to the time-step constraint to prevent occurrence of overtaking in computational particles:

$$\Delta t \le \frac{x^n_{R^\pm} - x^n_{L^\pm}}{v^n_{L^\pm} - v^n_{R^\pm}} \quad \text{if} \quad v^n_{L^\pm} > v^n_{R^\pm}. \tag{19b}$$

This condition will be taken as a constraint in the determination of the current time step. Once a shock is detected, these participating particles will be transformed to be shock particles to represent the peculiar dual states associated with the shock. However, the interpolated characteristic behind the shock must be modified to satisfy the Rankine–Hugoniot relation, Equation (15). A shock particle will move according to the shock speed rather than along with the characteristic lines as a regular particle:

$$x^{n+1}_s = x^n_s + \sigma^n \Delta t \tag{20}$$

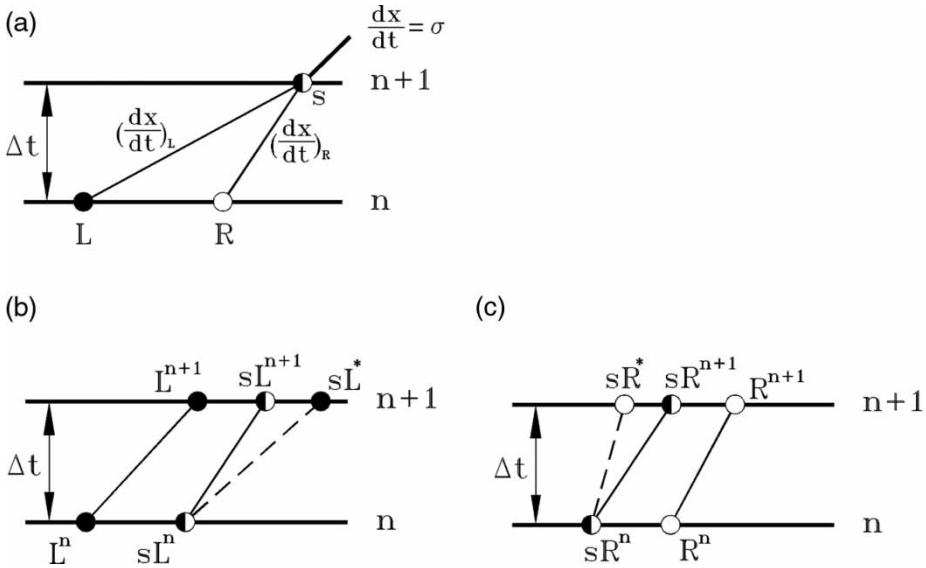

Figure 3 | Characteristics of a shock node: (a) formation; (b) left state; (c) right state.

where subscript s signifies a shock particle. The shock speed is also derived from the Rankine–Hugoniot relation, Equation (14):

$$\sigma = \frac{e^{h_L}v_L - e^{h_R}v_R}{e^{h_L} - e^{h_R}} \quad \text{or} \quad \sigma = \frac{e^{h_L}v_L^2 + e^{h_L} - e^{h_R}v_R^2 - e^{h_R}}{e^{h_L}v_L - e^{h_R}v_R}. \tag{21}$$

Since a shock particle moves with the shock speed and its resulting trail may not happen to be a characteristic line, the compatibility Equation (12) is not applicable to determine its transmitted characteristic. Alternatively, an appropriate interpolation must be taken to determine the transmitted characteristics before and after the shock. As illustrated in Figure 3(b), the transmitted characteristic $w_{sL^+}^{+,n+1}$ after the shock can be acquired from those at neighboring particles, $w_{L^+}^{+,n+1}$ and $w_{sL^*}^{+,n+1}$, with a linear approximation between these two nodes:

$$w_{sL^+}^{+,n+1} = \frac{(x_{sL^*}^{n+1} - x_{s^+}^{n+1})w_{L^+}^{+,n+1} + (x_{s^+}^{n+1} - x_{L^+}^{n+1})w_{sL^*}^{+,n+1}}{x_{sL^*}^{n+1} - x_{L^+}^{n+1}} \tag{22a}$$

where sL^* denotes the virtual state if the left-side shock particle moves as a regular one:

$$x_{sL^*}^{n+1} = x_{s^+}^{n} + (v_{sL^+}^{n} + 1)\Delta t \quad \text{and}$$
$$w_{sL^*}^{+,n+1} = (w_{sL^+}^{+,n} - w_{sL^+}^{-,n})e^{-\lambda\Delta t/\sqrt{2}} + w_{sL^+}^{-,n}$$

It is noted that the virtual node will move across the shock since $v_{sL^+}^{n} + 1 > \sigma$ for an admissible shock.

Similarly, as shown in Figure 3(c), the transmitted characteristic before the shock $w_{sR^+}^{+,n+1}$ can be obtained as:

$$w_{sR^+}^{+,n+1} = \frac{(x_{s^+}^{n+1} - x_{sR^*}^{n+1})w_{R^+}^{+,n+1} + (x_{R^+}^{n+1} - x_{s^+}^{n+1})w_{sR^*}^{+,n+1}}{x_{R^+}^{n+1} - x_{sR^*}^{n+1}}. \tag{22b}$$

The virtual right-side shock particle with subscript sR^* reads:

$$x_{sR^*}^{n+1} = x_{s^+}^{n} + (v_{sR^+}^{n} + 1)\Delta t \quad \text{and}$$
$$w_{sR^*}^{+,n+1} = (w_{sR^+}^{+,n} - w_{sR^+}^{-,n})e^{-\lambda\Delta t/\sqrt{2}} + w_{sR^+}^{-,n}.$$

It is also noted that its location will be lagged behind the shock.

As for the interpolated characteristics, the one ahead of the shock can be determined from the interpolation as its transmitted counterpart:

$$w_{sR^+}^{-,n+1} = \frac{(x_{s^+}^{n+1} - x_{sR^*}^{n+1})w_{R^+}^{-,n+1} + (x_{R^+}^{n+1} - x_{s^+}^{n+1})w_{sR^*}^{-,n+1}}{x_{R^+}^{n+1} - x_{sR^*}^{n+1}}. \tag{22c}$$

However, that behind the shock must be secured with the Rankine–Hugoniot relation in Equation (15). Evolution

of a left-running shock can be handled in the same manner. Once the states at the shock particles have been determined, they can be employed as internal moving boundary nodes to proceed with the simulation. In this sense, locations of shocks are explicitly detected without any intermediate nodes, which can be categorized as a shock-fitting procedure.

Particle management

In the present PMOC, the computational particles are maneuvered to move with transmitting velocity, which is heavily dependent upon the local flow condition. Therefore, the relative location between two successive particles may vary dramatically in the course of a computation. They may be divaricating due to the existing expansion fans or agglomerated by the compression shocks. Meanwhile, a particle may move across the computational boundary in which the special treatments to put up predefined boundary conditions must be taken into account. Consequently, several important issues concerning the management of computational particles must be clarified to ensure an effective simulation:

1. Time-step restriction mentioned in Equation (19b) is utilized to prevent the occurrence of overtaking between two successive particles. It is equally applied for the regular as well as shock particles of the same type.
2. Two agglomerated regular particles will be transformed as shock ones to characterize the associated shock structure. They will be imposed with dual states for the fulfillment of the Rankine–Hugoniot relation in Equation (15).
3. A regular particle merging with a shock one will be removed from the subsequent calculation. For concrete demonstration, this scenario is depicted in Figure 4(a) for a right-running particle.
4. A regular particle is also removed if it moves across a shock particle of a different type. Figure 4(b) shows the case of a left-running regular node move across a right-running shock one.
5. To ensure a sufficient number of computational particles to resolve flow features, a particle is inserted when two successive ones are separated with a distance larger than a prescribed value. As depicted in Figure 4(c), the inserted particle is assigned with the following attributes:

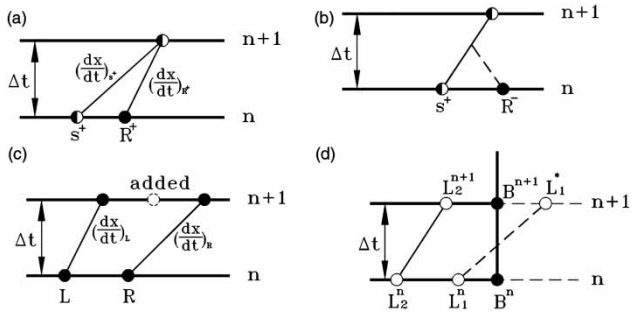

Figure 4 | Particle management: (a) removal of a regular particle; (b) removal of a computational particle; (c) addition of a computational particle; (d) treatment of a boundary node.

$$x_{in^+} = \frac{x_{L^+} + x_{R^+}}{2},\ w^-_{in^+} = \frac{w^-_{L^+} + w^-_{R^+}}{2} \quad \text{and}$$
$$w^+_{in^+} = w^-_{in^+} + (v_{L^+} + v_{R^+})/\sqrt{2}, \tag{23}$$

if $x_{R^+} - x_{L^+} \geq \delta_{\min}$. In the above relations, subscript *in* denotes the inserted particle and $\delta_{\min}$ is the assigned length scale to resolve flow features. Similar treatment will be applied for left-running particles.

6. A particle is simply removed if it moves across the computational domain. However, its transmitted characteristic can be used to derive the numerical boundary condition for the boundary node. As indicated in Figure 4(d), computational node L_1 will be removed since it moves across the boundary $\left(x_{L_L^*} > x_B\right)$. Nevertheless, the right-running characteristic at the boundary particle can be determined by assuming a linear distribution between nodes, L_1 and L_2:

$$w_B^{+,n+1} = \frac{\left(x_B^{n+1} - x_{L_2}^{n+1}\right) w_{L_1}^{+,*} + \left(x_{L_1}^{*} - x_B^{n+1}\right) w_{L_2}^{+,n+1}}{\left(x_{L_1}^{*} - x_{L_2}^{n+1}\right)}. \tag{24a}$$

The left-running characteristic at the boundary node can then be derived from the prescribed boundary condition. For example, if the piezometric head (h_B) or flow velocity (v_B) is given as the physical boundary condition, the left-running characteristic becomes:

$$w_B^{-,n+1} = \sqrt{2}h_B^{n+1} - w_B^{+,n+1} \text{ or } w_B^{-,n+1} = w_B^{+,n+1} - \sqrt{2}v_B^{n+1}, \tag{24b}$$

respectively. Conditions at the left boundary can be handled in the same manner.

In addition to the above particle management tactics, more versatile treatments can be considered to increase simulation effectiveness. For instance, the resolution scale for flow features $\delta_{\min}$ can be assigned in accordance with the local flow condition. It will yield an adaptive solution strategy in the account of solution efficiency. Meanwhile, clustered computational nodes with insignificant solution variations may be removed to economize the computational load.

Solution procedure

The numerical treatments in the above derivations are put into practice with the following steps:

1. Set up the initial conditions for all computational particles.
2. Calculate the time step with Equation (19b) to avoid particle overtaking.
3. Calculate the particle positions according to Equations (17) and (20) for regular and shock nodes, respectively.
4. Update nodal identity and transmitted characteristics.
5. Remove particle crossing shocks or computational domain.
6. Update the interpolated characteristics.
7. Update the flow conditions at boundary nodes.
8. Add regular particles in regions with deficient distribution.
9. Calculate transmitting velocity for all computational nodes.
10. Go to Step 2 until the assigned stop criterion has been met.

Since a computational particle may be added or removed in the computational course, a linked-list is adopted to record all particle information for computational convenience.

VALIDATION

Two categories of test problems with various unsteady flow characteristics are numerically solved to validate the present proposition. The first group comprises four problems with negligible convection term, which can then be analytically solved with series solutions (Sobey 2002, 2004). The second group emphasizes the effects of nonlinear convection terms which will induce strong pressure waves accompanied by expansion fans or shocks. Computations are also verified with available exact solutions as well as those obtained with a high-resolution finite volume (FV) method (Hwang & Chung 2002). As mentioned in the particle management section, computational time step is assigned to prevent occurrence of particle overtaking, and an adaptive particle addition and removal strategy is adopted to economize the computational effort with sufficient accuracy.

Problems with negligible convection term

The governing Equations (1) or (5) can be simplified to become a linear form if the nonlinear convection is omitted. Consequently, it can then be analyzed with series solutions based on the principle of superposition. These problems are raised and analytically solved by Sobey as testing benchmarks for numerical methods (Sobey 2004). The general analytical solution for piezometric head can be summarized as:

$$\begin{aligned} h(x,t) = {} & mx + b + a_1 exp(-\mu x) cos(kx - \omega t + \phi_1) \\ & + a_2 exp(+\mu x) cos(kx + \omega t + \phi_2) \\ & + \left[\hat{f}_0 + \frac{\hat{g}_0}{\lambda}(1 - exp(-\lambda t)) \right. \\ & \left. + \frac{1}{\lambda}\int_0^t (1 - exp(-\lambda(t-\tau)))\psi_0 d\tau \right] X_0(x) \\ & + \sum_{n=1}^{\infty} [\hat{f}_n exp(-\lambda t/2) cos(\omega_n t) \\ & + \frac{\hat{g}_n + \lambda \hat{f}_n/2}{\omega_n} exp(-\lambda t/2) \sin(\omega_n t) \\ & + \int_0^t \frac{1}{\omega_n} exp(-\lambda(t-\tau)/2) \sin \omega_n (t-\tau) \psi_n d\tau] X_n(x) \end{aligned} \tag{25}$$

Physical interpretations and definitions of solution parameters can be found in Sobey's work (Sobey 2004) and will not be repeated here for brevity. The solution for flow

velocity can be expressed with similar forms. Computations in the present study are performed by retaining the convection term and the results are compared with the linearized analytical solutions. All calculations are carried out in the region of $0 \leq x \leq 1$ and $t \geq 0$ with friction factor, $\lambda = 0.1$.

Sudden valve closure

The initial condition (IC) and boundary condition (BC) for this case are given as:

$$\text{IC: } h(x, 0) = h_0(1 - x) \quad \text{and} \quad v(x, 0) = v_0, \tag{26a}$$

$$\text{BC: } h(0, t) = h_0 \quad \text{and} \quad v(1, t) = \begin{cases} v_0 & t < t_0 \\ 0 & t \geq t_0 \end{cases}, \tag{26b}$$

where the head at reservoir is $h_0 = 10^{-4}$, the initial flow velocity $v_0 = h_0/\lambda$, and valve closure time $t_0 = 0.4$. This is a classic water-hammer problem in testing the numerical schemes. The initial condition depicts a steady velocity $v = v_0$ flowing from the reservoir at $x = 0$ to the exit at $x = 1$. The corresponding distribution of piezometric head can be deduced from momentum Equation (5b) with $dh/dx = -\lambda v_0$. At time $t = t_0$, the valve at the exit is suddenly closed which will induce a change in piezometric head propagating backward to the reservoir. Behind this wave, the original flowing fluid will become almost stagnant to cope with the boundary condition at the exit. When the wave reaches the reservoir, a reflected wave is created and propagates toward the exit, which also induces a reverse fluid flow ($v < 0$). A second reflected wave propagating toward the reservoir occurs as the wave arrives at the exit and the fluid will become almost stagnant behind the wave. Finally, a forward-moving wave is established as the wave hits the reservoir again, but the fluid behind the wave will flow towards the exit as in the initial condition ($v > 0$). These wave patterns will be repeated with a period of $T = 4$ but the wave strength will be weakened by action of fluid friction.

The above scenario can be simulated by the present formulation and the computational results are illustrated in Figures 5(a) and 5(b) for head and velocity wave patterns, respectively. As shown in these figures, the wave strength is effectively maintained without being smeared artificially by the numerical diffusion, which is inevitable for a fixed-grid finite-volume method (Hwang & Chung 2002) or MOC violating CFL constraint. The calculations are conducted with 200 initial computational nodes. Figure 6(a) demonstrates the simulation results as well as analytical solution distributions at $t = 0.2$, 0.6, 0.8, and 1.0 to depict the wave propagation characteristics. The analytical solutions are obtained with 200 terms in the sum in Equation (25). Very good agreement between the results of the present method and analytical solution are achieved, although the analytical solution shows some non-physically oscillation near the wave front. Comparisons of computational results with analytical solutions at $x = 0.1$, 0.3, 0.5, and 0.7 are illustrated in Figure 6(b). It clearly shows the present formulation can accurately mimic the flow transient phenomenon due to sudden valve closure.

Valve closure over finite time

This problem explores the response to valve closure from t_0 sinusoidally over a duration t_C. The initial and boundary conditions are assigned as:

$$\text{IC: } h(x, 0) = h_L x \quad \text{and} \quad v(x, 0) = v_0, \tag{27a}$$

$$\text{BC: } v(0, t) = \begin{cases} v_0 & \text{for } t \leq t_0 \\ \dfrac{v_0}{2}\left[1 + \cos\dfrac{\pi(t - t_0)}{t_c}\right] & \text{for } t_0 < t < t_0 + t_c \\ & \text{and } h(1, t) = h_L. \\ 0 & \text{for } t \geq t_0 + t_C \end{cases} \tag{27b}$$

It is worth noting that a reservoir with piezometric head h_L is located at right end ($x = 1$) and the valve is placed at left end ($x = 0$). The initial condition is a steady flow with uniform velocity $v_0 = -h_L/\lambda$. Calculations are carried out with the head at the reservoir being $h_L = 10^{-4}$ and the valve starting closure time is $t_0 = 0.4$. Figures 7(a), 7(b) and 7(c) show the solution evolution at various locations for, $t_C = 1.0$, 3.0, and 5.0, respectively. It clearly shows that the wave strength is successfully attenuated by increasing the valve closure duration time. As compared with analytical solutions, the present formulation yields very

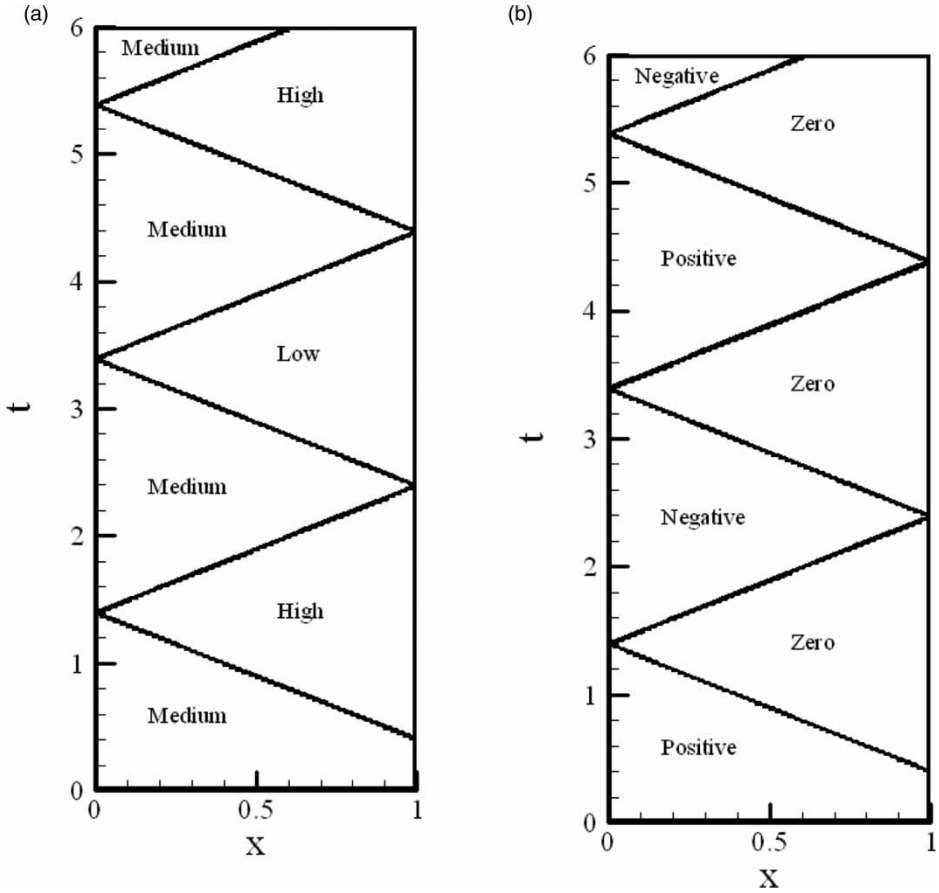

Figure 5 | Wave patterns in a sudden valve closure: (a) head; (b) flow.

agreed results for all the considered valve closure duration times.

Flow start-up

This problem considers the transient procedure of initially stagnant fluid evolving to steady state by opening a downstream valve. The associated initial and boundary conditions read:

$$\text{IC: } h(x, 0) = h_0 \quad \text{and} \quad v(x, 0) = 0, \tag{28a}$$

$$\text{BC: } h(0, t) = h_0 \quad \text{and} \quad h(1, t) = \begin{cases} h_0 & t < t_0 \\ 0 & t \geq t_0 \end{cases}. \tag{28b}$$

Boundary conditions at both ends are assigned with piezometric head. Calculations are carried out with the head at the reservoir being $h_0 = 10^{-4}$ and the valve opening time is $t_0 = 0.4$. Comparisons of computational results with analytical solutions for $x = 0.3$ and 0.7 are given in Figure 8. It clearly shows the flow evolving into steady state in a stepwise manner, which is driven by the wave propagation process. The head at two observed positions deviates due to the friction effect and the flow velocity asymptotically approaches the steady-state solution. Again, the present method can provide very accurate predictions as revealed in the comparison with analytical solutions.

Periodic forcing

This problem explores the unsteady response to a sudden periodic forcing in the reservoir at $x = 0$. The associated

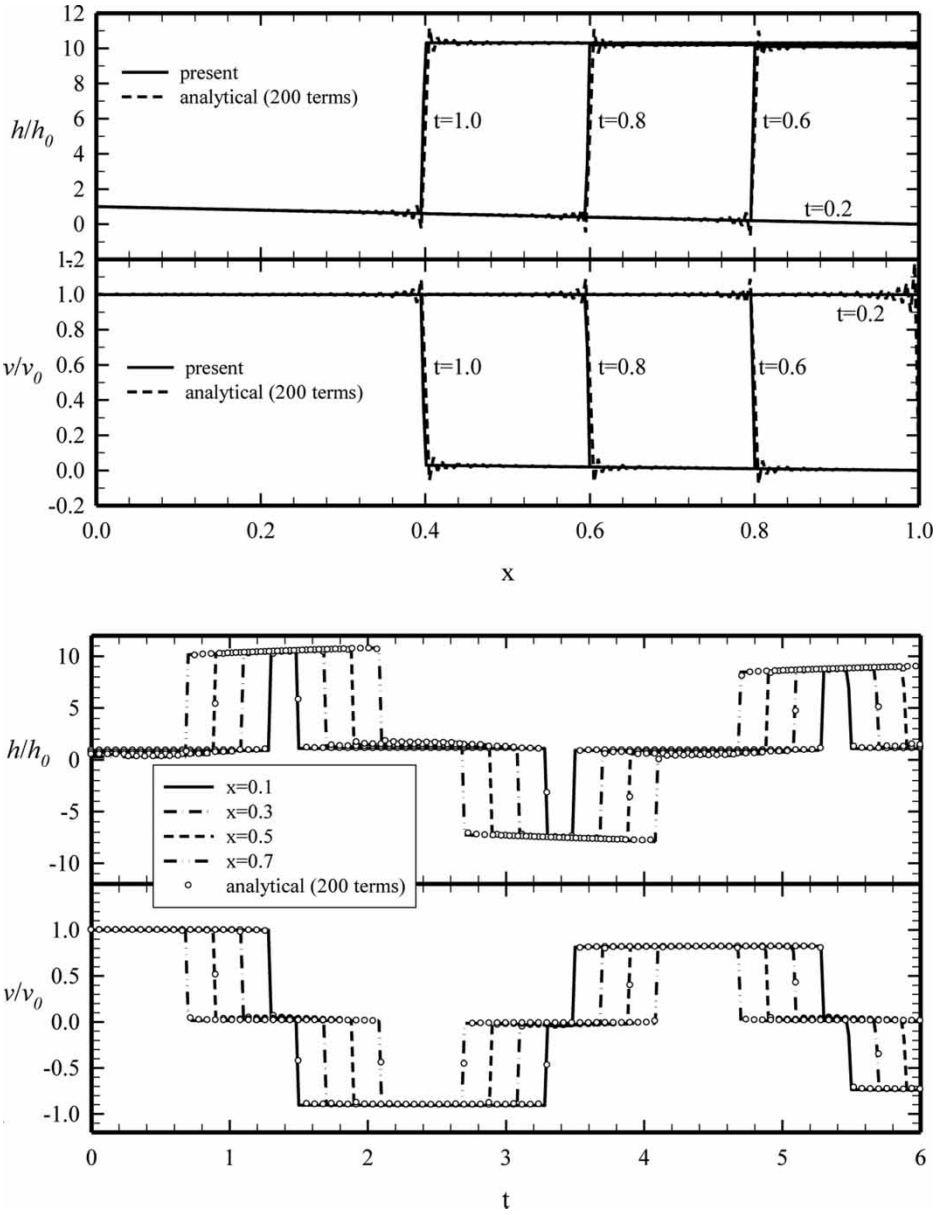

Figure 6 | Computational results in sudden valve closure problem.

initial and boundary conditions read:

$$\text{IC: } h(x, 0) = h_0(1 - x) \quad \text{and} \quad v(x, 0) = v_0, \tag{29a}$$

$$\text{BC: } h(0, t) = h_0 + a_0 \sin(\omega t) \quad \text{and} \quad h(1, t) = 0 \tag{29b}$$

In this problem, the initial piezometric head at the reservoir is $h_0 = 10^{-4}$ and the steady flow velocity is $v_0 = h_0/\lambda$. A sinusoidal variation in piezometric head at the reservoir is assigned to drive the unsteady flow field. The amplitude and frequency of this periodic forcing are $a_0 = 10^{-5}$ and $\omega = \pi/6$, respectively. Figure 9 illustrates the piezometric head and flow velocity response at various locations from the computational results as well as the analytical solutions. As shown in this figure, a sinusoidal variation is imposed upon the piezometric head but with diminishing magnitude toward the exit. In contrast to that flow velocity varies with nearly the same magnitude at all locations. There is also a

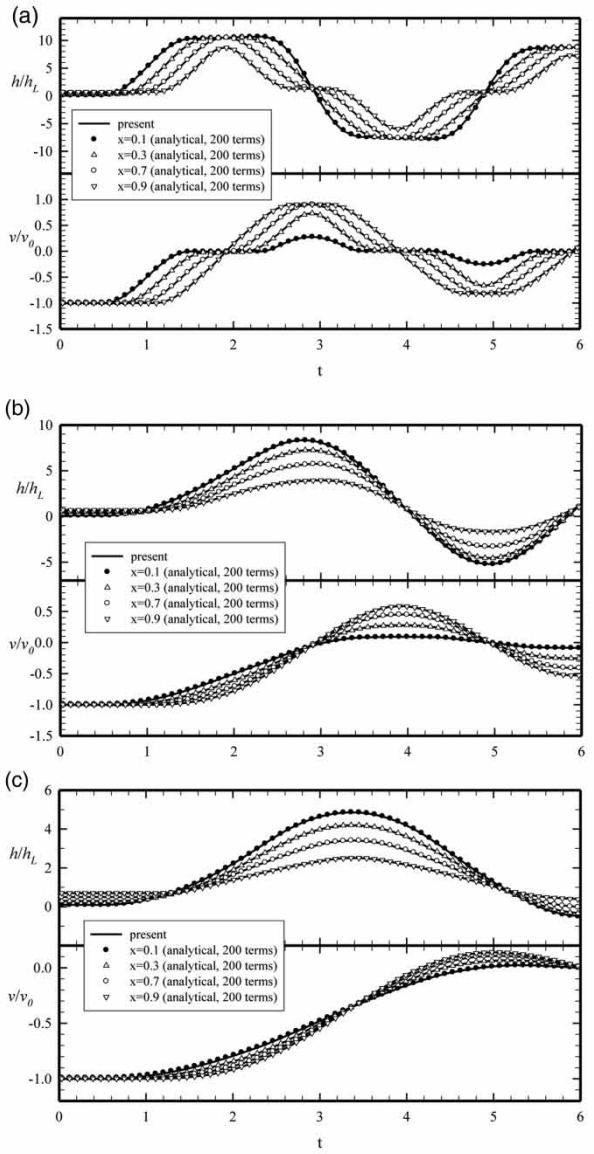

Figure 7 | Computational results in a valve closure over finite time problem: (a) $t_C = 1.0$; (b) $t_C = 3.0$; (c) $t_C = 5.0$.

phase difference between the head and velocity variations. These phenomena are closely replicated by the present method, which provides a very good agreement with the analytical solution.

Problems with significant convection term

The above validations are conducted with negligible convection term ($v \ll 1$), which can then be approximated with a linear equation system. All waves are almost propagating

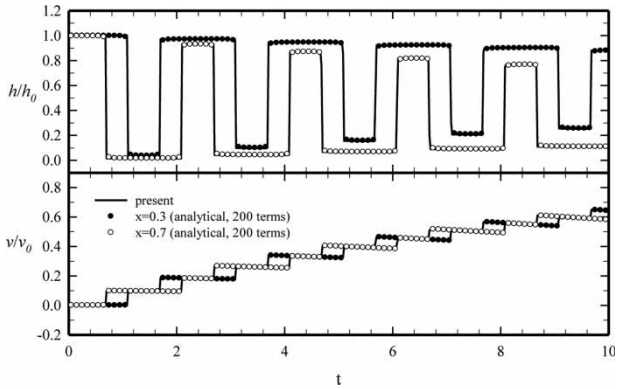

Figure 8 | Computational results in a flow start-up problem.

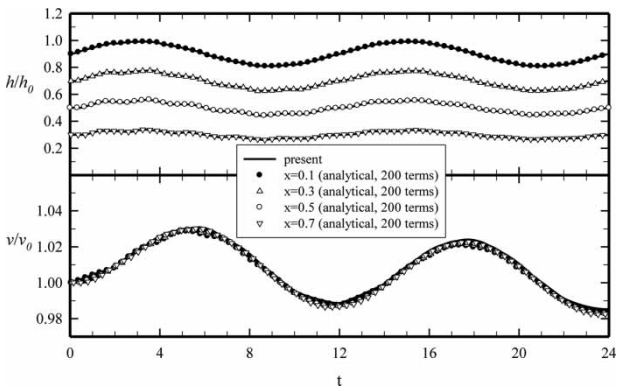

Figure 9 | Computational results in a periodic forcing problem.

with sound speed and the interactions between characteristic lines become insignificant. However, in the case with notable convection term, the transmitting velocity of flow characteristics will be dependent upon local flow condition. Wave interactions become inevitable in this circumstance, which is unable to be simulated with a linearized system or by a conventional MOC. For example, consider the case of sudden valve closure problem but with higher flow velocity, $v_0 = 0.1$. The computational results for waveform in $x - t$ plane and the resulting solution distributions at various times are demonstrated in Figures 10(a) and 10(b), respectively. As shown in these figures, a compression (expansion) wave will rebound as an expansion (compression) one as it reaches the reservoir at $x = 0$. These phenomena cannot be replicated with the linearized analysis or by a conventional MOC. Therefore, it is of essential importance to verify a numerical scheme in this situation.

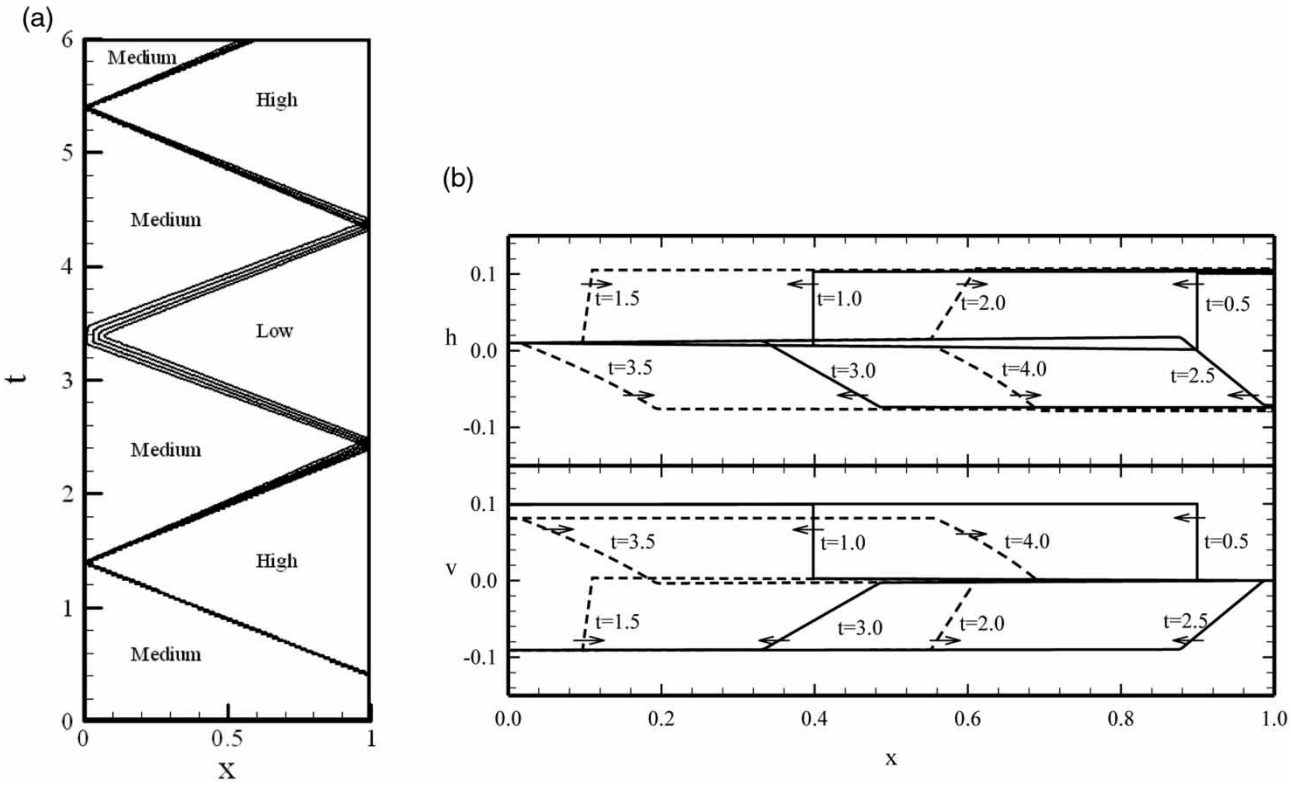

Figure 10 | Computational results in a sudden valve closure with $v_0 = 0.1$: (a) wave pattern; (b) solution distribution.

Inclusion of the nonlinear convection term will create substantial hurdles in the transient analysis of pipe flows. Exact solutions are not amenable except in some simplified cases. Therefore, we consider some standard shock tube problems whose exact solutions are achievable with similarity transformation (Hirsch 1990; Hwang & Chung 2002). In a shock tube problem, two distinct states of (h_L, v_L) and (h_R, v_R) are initially separated by a diaphragm in a pipeline. At $t = 0$, the diaphragm is suddenly ruptured, which will yield expansion or compression waves evolving into the initially uniform regions. Meanwhile, an intermediate state will emerge between these waves. Wave patterns and the associated exact solutions can be derived from the compatibility equations combined with the Rankine–Hugoniot relation (Hirsch 1990; Hwang & Chung 2002).

Three cases with different wave patterns are considered. All calculations are conducted in the region of $0 \le x \le 1$ with initially a uniform 40 computational nodes. The initial dividing diaphragm is located at $x = 0.5$. The first test problem is proposed with the following initial states:

$$(h_L, v_L) = (2, 0) \quad \text{and} \quad (h_R, v_R) = (1, 0). \tag{30a}$$

With these initial states, a compression wave will develop propagating into the right region ($x > 0.5$) and an expansion one into the left region ($x < 0.5$) which can be deduced from the characteristic relations (Hwang & Chung 2002):

$$2\sinh(\varepsilon_h/2) - \varepsilon_v > 0 \quad \text{and} \quad \varepsilon_h + \varepsilon_v > 0. \tag{30b}$$

The intermediate state can be secured by the following relations:

$$2\sinh\left(\varepsilon_h^*/2 + \varepsilon_h/4\right) + \varepsilon_h^* = \varepsilon_v + \varepsilon_h/2 \quad \text{and} \quad \varepsilon_v^* = \varepsilon_v/2 + \varepsilon_h/2 - \varepsilon_h^*/2, \tag{30c}$$

which will yield $h^* = 1.4974$ and $v^* = 0.5026$. In the above equations, some solution parameters are introduced for

convenience:

$$\varepsilon_h = h_L - h_R,\ \varepsilon_v = v_L - v_R,\ \varepsilon_h^* = h^* - (h_L + h_R)/2 \quad \text{and} \quad \varepsilon_v^* = v^* - (v_L + h_R)/2$$

where the superscript * denotes the intermediate state. The computational results at $t = 0.2$ and 0.5 with the present method are shown in Figure 11(a), where exact solutions as well as those obtained with a high-resolution FV method (Hwang & Chung 2002) are also included for comparison. As illustrated in this figure, very accurate results can be obtained with the proposed PMOC and the FV method yield smeared results across the shock and expansion waves.

The second problem is assigned with the following initial states:

$$(h_L, v_L) = (1, 0) \quad \text{and} \quad (h_R, v_R) = (1, -1). \tag{31a}$$

It will develop two compression waves evolving into both the left and right regions since the following characteristic relations prevail (Hwang & Chung 2002):

$$2\sinh(\varepsilon_h/2) - \varepsilon_v < 0 \quad \text{and} \quad 2\sinh(\varepsilon_h/2) + \varepsilon_v > 0. \tag{31b}$$

Accordingly, the intermediate state can be secured:

$$\varepsilon_h^* = 2\sinh^{-1}[\varepsilon_v/4\cosh(\varepsilon_h/4)] \quad \text{and} \quad \varepsilon_v^* = 2\cosh(\varepsilon_h^*/2)\sinh(\varepsilon_h/4), \tag{31c}$$

which will yield $h^* = 1.4949$ and $v^* = -0.5$ in this case. The computational results as well as the exact solutions at $t = 0.2$ and 0.5 are depicted in Figure 11(b). As compared with FV, it clearly shows that the present PMOC can provide very accurate results with the exact solutions.

The final problem in this category is considered by the following initial states:

$$(h_L, v_L) = (1, -1) \quad \text{and} \quad (h_R, v_R) = (1, 0). \tag{32a}$$

It will develop two expansion fans evolving into both the left and right regions since the following characteristic relations prevail (Hwang & Chung 2002):

$$\varepsilon_h + \varepsilon_v < 0 \quad \text{and} \quad \varepsilon_h - \varepsilon_v > 0. \tag{32b}$$

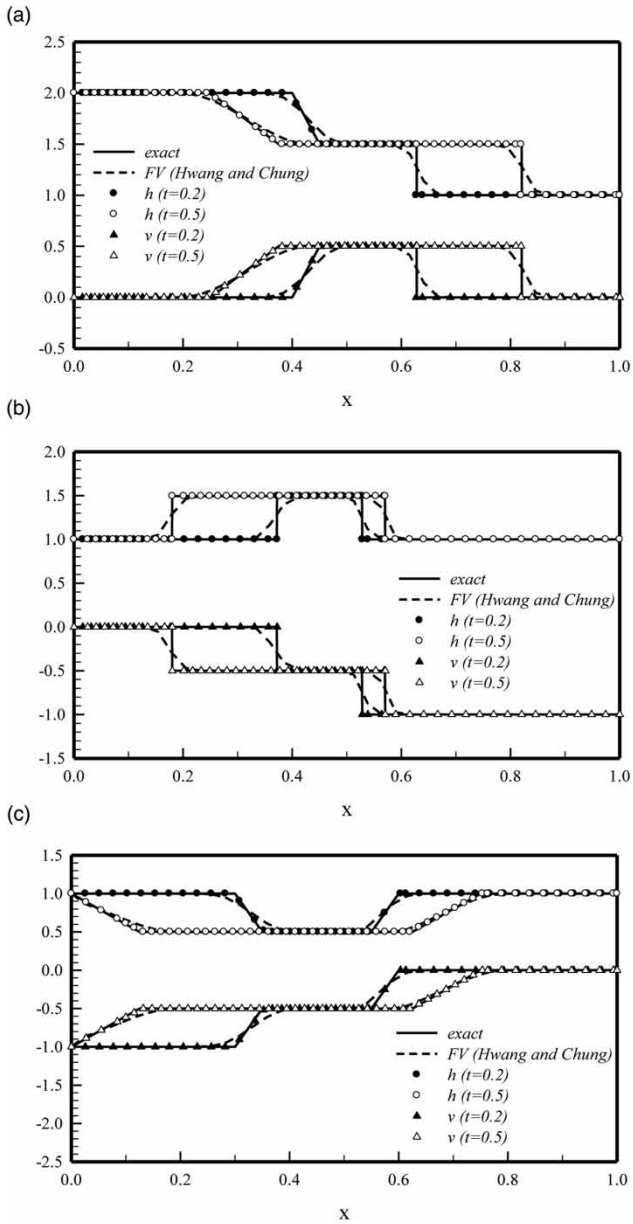

Figure 11 | Computational results in shock-tube problems: (a) $(h_L, v_L) = (2, 0)$ and $(h_R, v_R) = (1, 0)$; (b) $(h_L, v_L) = (1, 0)$ and $(h_R, v_R) = (1, -1)$; (c) $(h_L, v_L) = (1, -1)$ and $(h_R, v_R) = (1, 0)$.

The intermediate state can be obtained:

$$\varepsilon_h^* = \varepsilon_v/2 \quad \text{and} \quad \varepsilon_v^* = \varepsilon_h/2, \tag{32c}$$

which will yield $h^* = 0.5$ and $v^* = -0.5$ in this case. Figure 11(c) shows the computational results and the associated exact solution at $t = 0.2$ and 0.5. Again, very accurate

results can be obtained with the present formulation. Finally, Figure 12 demonstrates the resulting intermediate states ($h^* - h_R$ and v^*) and shock locations at $t = 0.2$ for initial state of $(h_L, 0)$ and $(h_R, 0)$ with $0 \leq h_L - h_R \leq 8$. It clearly indicates that the exact solutions are truthfully replicated by the present PMOC.

As for the required computer resource to accomplish a simulation, the present particle method may induce much heavier computational load than a FV method since it demands more complicated manipulations in handling wave interactions explicitly. In fact, almost 20-fold of computational time is entailed by the characteristic particle method as compared with a FV method in our programming. Nevertheless, it may attain quite excellent simulation to compensate the excessive computational load. Furthermore, the required computational load is not such a serious issue in one-dimensional problems as in multi-dimensional ones.

CONCLUSIONS

A comprehensive and useful numerical method to simulate unsteady pipe flows is proposed and validated in the present work. It is built based on the compatibility equations derived from the governing equation system. Contrary to the conventional MOC, two groups of particles are employed to take care of two transmitted characteristics. The computational particles are managed to follow their individual characteristic lines. In this manner, the cumbersome CFL constraint in the conventional MOC can be effectively eradicated. Therefore, the present proposition is coined as a PMOC.

Besides the regular particles to tackle flow characteristics, supplementary shock particles with dual states are imposed to imitate the admissible shock structure. They are introduced with the fulfillment of Rankine–Hugoniot relations. The shock location and its propagation speed can then be specified without numerical ambiguity. Validations of the present formulation are performed by solving some benchmark problems with significant transient effects. The computational results are compared with available analytical or exact solutions to depict their accuracy. From the derivation procedure and the obtained numerical results, one can conclude that the present PMOC will be a useful tool to simulate unsteady pipe flows.

Although the proposed method and the associated test problems in the present study are confined in a single pipeline, it can easily be extended for simulation of transients in pipe networks if the junction conditions with multiple branches are appropriately resolved. It can be achieved with the characteristics propagation given in the compatibility Equations (12a) and (12b). For example, the numerical conditions for piezometric head and flow velocity in a junction with three branches, shown in Figure 13, can be summarized as:

$$\frac{Hg}{a_1^2} + \frac{V_1}{a_1} = w_1^+, \ \frac{Hg}{a_2^2} + \frac{V_2}{a_2} = w_2^+, \ \frac{Hg}{a_3^2} + \frac{V_3}{a_3} = w_3^+ \quad \text{and}$$

$$V_1 D_1^2 + V_2 D_2^2 + V_3 D_3^2 = 0$$

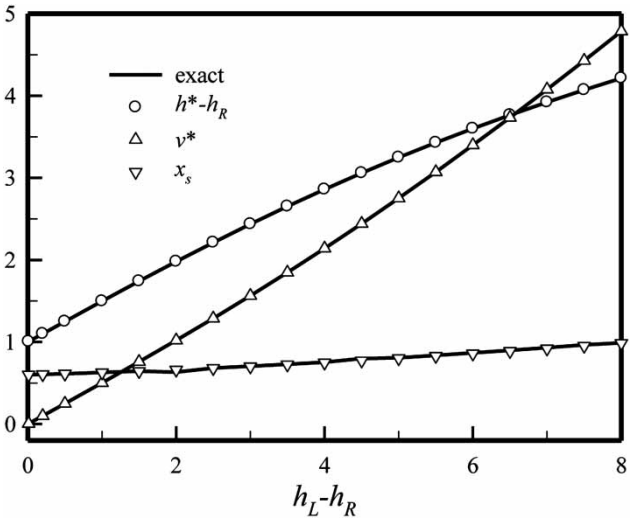

Figure 12 | Intermediate states and shock locations in shock-tube problems at $t = 0.2$.

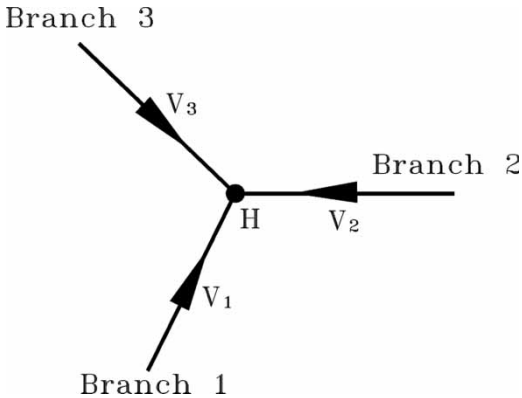

Figure 13 | Treatment of a junction with three branches.

where w_i^+ is incoming characteristic in i-th branch, which can be obtained from the compatibility equations. The last equation is the mass continuity equation assuming that there is no mass addition or removal at the junction. Therefore, there are four equations to determine the four unknown ones associated with the junction (H, U_1, U_2, and U_3). Further investigation on this topic is in progress and the results will be reported in the near future.

REFERENCES

Abbott, M. B. 1966 *An Introduction to the Method of Characteristics*. Thames and Hudson, London.

Carnaha, B., Luther, H. A. & Wilkes, J. O. 1969 *Applied Numerical Methods*. John Wiley & Sons, New York.

Chaudhry, M. H. 1987 *Applied Hydraulic Transients*. Van Nostrand Reinhold, New York.

Ghidaoui, M. S. & Karney, B. W. 1994 Equivalent differential equations in fixed-grid characteristics method. *J. Hydraul. Eng.* **120**, 1159–1176.

Ghidaoui, M. S., Zhao, M., McInnis, D. A. & Axworthy, D. H. 2005 A review of water hammer theory and practice. *Appl. Mech. Rev.* **58**, 49–76.

Gingold, R. A. & Monaghan, J. J. 1977 Smoothed particle hydrodynamics – theory and application to non-spherical stars. *Mon. Not. R. Astron. Soc.* **118**, 357–389.

Goldberg, D. E. & Wylie, E. B. 1983 Characteristics method using time-line interpolations. *J. Hydraul. Eng.* **109**, 670–683.

Hirsch, C. 1990 *Numerical Computation of Internal and External Flows, Vol. 2: Computational Methods for Inviscid and Viscous Flows*. Wiley, New York.

Hwang, Y.-H. 2011 A moving particle method with embedded pressure mesh (MPPM) for incompressible flow calculations. *Numer. Heat Transf. B* **60**, 370–398.

Hwang, Y.-H. & Chung, N.-M. 2002 A fast Godunov method for the water hammer problem. *Int. J. Numer. Methods Fluids* **40**, 799–819.

Lai, C. 1988 Comprehensive method of characteristics for flow simulation. *J. Hydraul. Eng.* **114**, 1074–1097.

LeVeque, R. J. 2002 *Finite Volume Methods for Hyperbolic Problems*. Cambridge Press, Cambridge.

Lister, M. 1960 The numerical solution of hyperbolic partial differential equations by the method of characteristics. In: *Numerical Methods for Digital Computer* (A. Ralsion & H. S. Wilf, eds.). Wiley, New York, pp. 165–179.

Shapiro, A. H. 1953 *The Dynamics and Thermodynamics of Compressible Fluid Flow*. John Wiley & Sons, New York.

Sibertheros, I. A., Holley, E. R. & Branksi, J. M. 1991 Spline interpolation for water hammer analysis. *J. Hydraul. Eng.* **117**, 1332–1351.

Sobey, R. J. 2002 Analytical solution of non-homogeneous wave equation. *Coast. Eng. J.* **44**, 1–24.

Sobey, R. J. 2004 Analytical solutions for unsteady pipe flow. *J. Hydroinformat.* **6**, 187–207.

Tullis, J. P., Streeter, V. L. & Wylie, E. B. 1976 Waterhammer analysis with air release. *Proc. 2nd Int. Conf. Pressure Surge*, BHRA, Bedford, UK.

van Leer, B. 1973 Towards the ultimate conservative difference scheme I. The quest of monotonicity. In: *Lecture Notes in Physics*. Vol 18, (H. Cabannes & R. Temam, eds). Springer-Verlag, Berlin, pp. 163–168.

Wiggert, D. C. & Sundquist, M. J. 1977 Fixed-grid characteristics for pipeline transients. *J. Hydraul. Div.* **103**, 1403–1415.

Wylie, E. B. & Streeter, V. L. 1976 One-dimensional soil transients by characteristics. *Proc. 2nd Int. Conf. Numerical Methods in Geomechanics*, VPI, Blacksburg, VA.

Wylie, E. B. & Streeter, V. L. 1993 *Fluid Transients in Systems*. Prentice-Hall, Englewood Cliffs, NJ.

Yang, J. C. & Hsu, E. L. 1991 On the use of the reach-back characteristics method for calculation of dispersion. *Int. J. Numer. Methods Fluids* **12**, 225–235.

First received 3 July 2012; accepted in revised form 13 November 2012. Available online 18 December 2012